Process monitoring during AlN_xO_y deposition by reactive magnetron sputtering and correlation with the film's properties

J. Borges[1], N. Martin[2], F. Vaz[1], L. Marques[1]

[1]Centro de Física, Universidade do Minho, Campus de Gualtar, 4710-057 BRAGA, PORTUGAL
[2]Institut FEMTO-ST, Département MN2S, UMR 6174 CNRS, Université de Franche-Comté, ENSMM, UTBM, 32, Avenue de l'Observatoire, 25044 BESANÇON Cedex, FRANCE

ABSTRACT

In this work, AlN_xO_y thin films were deposited by reactive magnetron sputtering, using an aluminum target and an $Ar/(N_2+O_2)$ atmosphere. The DC magnetron discharge parameters during the deposition process were investigated by optical emission spectroscopy and a plasma floating probe was used. The discharge voltage, the electron temperature, the ion flux and the optical emission lines were recorded for different reactive gas flows, near the target and close to the substrate. This information was correlated with the structural features of the deposits as a first step in the development of a system to control the structure and properties of the films during reactive magnetron sputtering. As the target becomes poisoned, the discharge voltage suffers an important variation, due to the modification of the secondary electron emission coefficient of the target, which is also supported by the evolution of the electron temperature and ion flux to the target. The sputtering yield of the target was also affected, leading to a reduction of the amount of Al atoms arriving to the substrate, according to optical emission spectroscopy results for Al emission line intensity. This behavior, together with the increase of non-metallic elements in the films, allowed obtaining different microstructures, over a wide range of compositions, which induced different electrical and optical responses of films.

I. INTRODUCTION

The research in the area of thin films is driven by the increasing demands of industry to find high-tech solutions that may solve the problems that limit the operation of certain coating systems in several kinds of devices.[1] Wear and corrosion in protective-like coating systems,[2-4] hardness and mechanical resistance in tools and machine parts,[5-7] structural stability in decorative consumer goods,[8,9] biocompatibility in prosthesis pressure sensors,[10] among several other examples. The most recent research shows that the development of systems that configure a multifunctional behavior, by proper selection of coating method, is of particular interest since they can offer a combination of properties in the same material.[11-14] Several physical vapor deposition (PVD) techniques have been applied with great success in several of the upper mentioned technological fields, due to a wide range of material combinations and the possibility to respond to a significant number of property requirements. Among them, the reactive magnetron sputtering process[15-19] is a widely used technique to deposit different kinds of compounds (oxides, nitrides, oxynitrides, oxicarbides, etc.),[20-26] since it offers a good relation cost/ quality of the final product.[27] For all these PVD processes, a rigorous and careful control of the processing conditions (discharge conditions, plasma composition, plasma parameters and deposition characteristics) is of fundamental importance, not only to produce the targeted thin film system with the desired characteristics (composition, structure, morphology, etc) and properties (electrical, optical, mechanical, etc), but also to establish some correlations between processing parameters and thin film characteristics/properties. This allows optimizing the deposition process in relation to the basic requirements of the desired application, as well as facilitating the transfer of technology to other deposition systems and/or to the industry.

The metallic oxynitrides (MeN_xO_y, Me= metal) are an important class of materials that gained importance in the last decade, due to their excellent physical, chemical and mechanical properties, which hold promising characteristics for a wide range of applications, including corrosion protection, wear resistance, decorative applications, optoelectronics, microelectronics, solar cells, high–*k* gate dielectrics, biomedical coatings, gas barriers, among others.[28] The relevance of the MeN_xO_y materials arises from the possibility of merging the benefits of the basic characteristics and properties of both metal nitrides and oxides, which are very important in many areas of technology.[21,23] There are several works related to the preparation of metallic oxynitrides

by sputter deposition from metallic targets (Ti, Zr, Hf, Nb, Ta, Cr, W, etc.), where it was demonstrated that by tuning the concentration of oxygen and nitrogen it is possible to tailor the films' properties between those of the nitrides (MeN_x) and those of the corresponding oxides (MeO_y).[24,29-36]

Another important metallic oxynitride system is the aluminum oxynitride (AlN_xO_y), since it offers the possibility to obtain a wide range of responses, included among those of the correspondent base systems: Al, AlN and Al_2O_3. The systematic study of this system is being carried out by these authors, who found some promising characteristics and responses, already discussed in some papers,[37-41] which are distinct from the well-known properties of the ceramic AlON material.[42-44] It was actually found that the electrical and optical responses of the AlN_xO_y films strongly depend on the composition, bonding characteristics and microstructure of the films. Nevertheless, in order to control the functional properties of the deposited films, it is important to understand the influence of the deposition conditions on the resulting microstructure and phase's composition.[45] For this purpose it becomes fundamental to monitor the characteristics of the plasma used as source of energetic ions and how it is affected by the external parameters (flux of reactive gas, pressure, target-substrate distance, current density). It is known that a change in a single parameter is capable of changing several other parameters (electron temperature, particles flux, plasma density).[45]

Taking the above as a starting point, this work is devoted to characterize an $Ar/(N_2+O_2)$ plasma generated by a DC magnetron discharge, during the deposition of AlN_xO_y films. The major concern was to study some basic plasma parameters as a function of the partial pressure of the reactive gas, such as electron temperature, ion flux and plasma density, linking these characteristics with the discharge voltage and deposition characteristics, and establish some correlations with the films' microstructure and properties.

II. MATERIALS AND METHODS

A. Deposition system

The experiments were conducted in a custom-made deposition system operating at a base pressure of 10^{-4} Pa, mainly composed of a cylindrical deposition chamber with a volume of 0.04 m^3, a vacuum system, a gas flow control system, an electrical system, a pre-chamber and a control

unit. The deposition chamber is formed by four vertically rectangular magnetrons (unbalanced of type 2), in a closed field configuration. Only one magnetron was used to produce the films, powered by a Hüttinger PFG 7500DC (maximum output of 7.5 kW). The primary vacuum of the chamber is obtained by two parallel rotary vane vacuum pumps, a TRIVAC D 8B (pumping speed of 2.36 L-s^{-1}) and a Balzers Duo 012A (3.3 L.s^{-1}). The secondary vacuum (with pressures of ~10^{-4} Pa) is obtained using a Turbo Molecular high vacuum pump from Alcatel, model PTM 5400 (400 L.s^{-1}).The gas atmosphere was composed of argon (working gas), with a partial pressure fixed at 3×10^{-1} Pa (70 sccm), and a reactive gas mixture composed of nitrogen and oxygen, with a constant N_2:O_2 ratio of 17:3. The gas flow is controlled by mass flow meters and it is injected uniformly in the chamber using a circular tube (with small holes) positioned in the chamber's inside wall. The plasma was generated by a DC magnetron discharge with an aluminum target (99.6% purity) having 200×100×6 mm^3dimensions. The DC current density was fixed at 75 A.m^{-2}. The chamber walls and the rotating substrate holder (located 70 mm from the cathode) were grounded and the latter was kept at a constant temperature (~100 ºC) before discharge ignition, by using a Joule effect resistor. Before each set of measurements, a target cleaning process was carried out in pure argon until the target voltage reached a steady state.

B. Monitoring the discharge parameters

1. The acquisition system

The target potential and discharge current, the flow of the gases, the partial pressures and the substrate temperature, were monitored using a Data Acquisition/Switch Unit Agilent 34970A, with a multifunction module (334907A). This unit uses a RS-232 interface and the data is acquired with Benchlink Data Logger III software. The power supply, the pressure sensors and the flow controllers have analog outputs, which allow the connections to the acquisition system. The substrate temperature was measured by a RTD (Resistance Temperature Detector), model Pt100 (JUMO Instruments Co. Ltd.), placed close to the silicon substrate. The partial pressure of the reactive gas was measured prior to discharge ignition, being directly proportional to the gas flow.

2. The floating probe

With the purpose of measuring some plasma parameters, a floating-type probe was installed in the deposition system. FIG. 1 shows a schematic diagram of the experimental setup. The system consists of a probe body (copper), connected in series with a DC blocking capacitor (C = 100 μF), and a current sensing resistor (R = 47 or 100 Ω). The dimensions of the probe tip, exposed to the plasma, were 12.5 mm in length and 1 mm in diameter.

In this kind of probe, an AC signal generator is used to apply a sinusoidal wave between the probe tip and the ground. The current from the plasma can flow through the probe even if a non-conducting film is deposited during processing. This allows its use in reactive atmospheres, where the well-know Langmuir probes are not adequate.[46] Due to nonlinear effects of the probe sheath, the measured current has several harmonics of the fundamental frequency.[47-49] The current flowing through the probe can be measured with a digital oscilloscope, from the voltage difference across the current sensing resistor. The intensities of the harmonics can be analyzed by Fast Fourier Transformation (FFT) of the output signal.[49]

It is possible to demonstrate that the ratio between the amplitudes of the first (i_{1f}) and second (i_{2f}) harmonics is given by:[46]

$$\frac{i_{1f}}{i_{2f}} = \frac{I_1(eV_0/T_e)}{I_2(eV_0/T_e)} \quad (1)$$

where T_e is the electron temperature (in eV), V_0 corresponds to the amplitude of the signal applied to the probe, and I_1 and I_2 are solutions of the modified Bessel function of the first kind, $I_n(x)$. Eq. 1 was deduced assuming that the electrons follow a Maxwell-Boltzmann distribution function [47]. The electron temperature can then be calculated from Eq. 1.

It is also possible to determine the ion flux to the probe using the following equation:[48]

$$\Gamma^+ = \frac{i_{1f}}{2}\frac{I_0(eV_0/T_e)}{I_1(eV_0/T_e)} \quad (2)$$

where I_0 is the zero order solution of the modified Bessel function of the first kind. After obtaining the electron temperature from Eq. 1 it's possible to determine the ion flux using Eq. 2.

The plasma density (n_i) can also be estimated by [48]:

$$n_i = \frac{\Gamma^+}{0.61\, v_B} \quad (3)$$

where, v_B represents the Bohm velocity, defined as the minimum velocity which the ions cross the probe sheath. It depends on the electron temperature and ion mass (M_i) according to:

$$v_B = \sqrt{\frac{k_B T_e}{M_i}} \quad (4)$$

The measurement of plasma parameters was made in two different positions: ~18 mm away from the race track of the target and at ~22 mm from the substrate holder (in static mode).

3. Optical emission spectroscopy (OES) measurements

The optical emission spectroscopy (OES) is a non-invasive method, which allows monitoring the chemical species present in the plasma[50] and, in some conditions, some plasma parameters such as electron temperature and plasma density can be obtained.[51-54]

In the present case, the optical emission spectra from the plasma were recorded over the 350-1100 nm wavelength range using an Ocean Optics - HR4000 Spectrometer, via a quartz optical fiber.

C. Characterization of the deposited films

The chemical composition of the films was investigated by Rutherford Backscattering Spectrometry (RBS). Measurements were made at 2 MeV with $^4He^+$ and 1.4 MeV with $^1H^+$, at normal incidence. There are three detectors in the chamber: one located at a 140º scattering angle respective to the beam direction, and two pin-diode detectors located symmetrically each other, both at a 165º scattering angle. The data were analyzed with the code NDF.[55]

The structure and the phase distribution of the films were analyzed by X-ray diffraction (XRD), using a PANalytical X'Pert PRO – MPD. The XRD patterns were deconvoluted, assuming to be Pearson VII functions, to yield the peak position, peak intensity and integral breadth, using Winfit software.[56]

Morphological features of the samples were probed by scanning electron microscopy (SEM), using a High resolution (Schottky) Environmental Scanning Electron Microscope with X-Ray Microanalysis and Electron Backscattered Diffraction analysis: Quanta 400 FEG ESEM /

EDAX Genesis X4M, operating at 15 keV. The thickness of the samples was estimated by cross-section SEM analysis and the growth rate was calculated by the ratio between the average thickness and the deposition time (90 min. for all samples).

III. RESULTS AND DISCUSSION

A. Target Potential

The evolution of the cathode potential as a function of the partial pressure of the reactive gas mixture (N_2+O_2) is plotted in FIG. 2. The equilibrium target potential varies almost linearly from a maximum value of 400 V, for an atmosphere without reactive gas, to a value of about 299 V when the reactive gas partial pressure is approximately 4.6×10^{-2} Pa. Then it sharply decreases to 259 V when the partial pressure of N_2+O_2 rises to 5.6×10^{-2} Pa, with no significant variation of the target potential thereafter. According to this brief analysis of the results, there are clearly two different regimes of the target, which were denoted in FIG. 2 as regime I, where the values of the cathode voltage gradually decrease, and as regime II, for approximately constant target potential values.

Although the target potential is a simple parameter to measure, it depends on several parameters such as the target condition, the magnetron configuration, the geometry of the chamber, the applied current, the gas pressure, just to mention a few.[57,58] It is also important to consider the influence of the reactive gas species, since they are not only used to form the film on the substrate, but can also interact with the target,[59] leading both to compound formation[60,61] at its surface and to ion implantation.[62]

In the particular case of magnetron sputtering of Al targets it was demonstrated that the target potential decreases as the partial pressures of reactive gases are increased, namely the cases of Ar/O_2[59,63,64] and Ar/N_2[63,65,66] discharges. To explain this behavior one has to keep in mind that the discharge sustaining mechanism is based on the emission of secondary electrons from the target during their Ar ion bombardment.[58] The number of emitted electrons is quantified by the effective secondary electron emission yield (γ_{eff}),[58] which is proportional to the (i) ion induced secondary electron emission (γ_{ISEE}) coefficient,[67] (ii) the effective gas interaction probability and (iii) a multiplication factor due to sheath ionization.[58] According to the results obtained by Depla et al., the effective emission coefficient of the Al target increases more than 100 % when nitridation or oxidation occurs.[58] Since γ_{eff} is inversely proportional to the minimum discharge voltage, the addition of reactive gases, such as oxygen and nitrogen, is expected to promote the

gradual oxidation/nitridation of the target and thus enhancing the number of secondary electrons. These modifications will have a strong influence on the target potential, which explains the behavior observed in the regime I of the target, FIG. 2.

Regarding the regime II, it is most likely that the target is totally covered by an Al based compound – an oxide-like film (target totally poisoned), which explains the nearly constant values of the target potential. Within the range of pressures ascribed to the regime II and for pressures above $5.6x10^{-2}$ Pa, it was also observed some instabilities during the discharge, due to arcing phenomena, which is a typical behavior in this kind of discharges, namely when the target is covered by a dielectric layer.[68,69]

Due to the target poisoned effect, the most relevant film's characteristics were found for partial pressures of the reactive gas up to $5.6x10^{-2}$ Pa, where it was obtained a wide range of compositions and different microstructures, which induced a gradient of properties, tailored between those of pure aluminum and those of aluminum nitride or oxide.[4,39,41] In order to better understand the behavior of the target with the increase of the partial pressure of the reactive gas up to $5.6x10^{-2}$ Pa, some plasma characteristics were studied by recording the optical emission lines of the plasma species and by measuring some basic plasma parameters using a plasma floating probe. This basic knowledge about the plasma will also allow establishing some correlations between the discharge conditions and the characteristics of the deposited films.

B. Optical emission spectroscopy

FIG. 3 shows optical emission spectra of the $Ar/(N_2+O_2)$ plasmas generated during the preparation of different AlN_xO_y thin films, resulting from different partial pressures of the reactive gas mixture (N_2+O_2), that were selected in the framework of the present study. As it can be observed, the spectra are dominated by transitions between the first two excited configurations of Ar I ($4p \rightarrow 4s$), and two lines of Al I corresponding to transitions from the first excited state to the ground state ($4s \rightarrow 3p$). Some of the lines are superimposed due to limitations of the equipment. It is noteworthy that emission lines related to transitions of nitrogen and oxygen species were not detected. This means that, most probably, the reactive gas is mainly used to form aluminum compounds on the chamber's surfaces, namely in the target, as discussed in the previous section, as well as on the substrates and chamber walls.

The main lines recorded from the Ar/(N_2+O_2) plasma are summarized in TABLE I. The diagram of the energy levels associated to the transitions mentioned in TABLE I can be observed in.[53]

The first important note about the set of results that were obtained is that the argon emission lines are typical of discharges at low pressure,[53,54,70] which result from some important processes that involve excited states of Argon: (i) the electron impact excitation of Ar from the ground state; (ii) the electron impact transition between exited levels and (iii) the spontaneous radiation emission.[71] The excited Ar species can also be depopulated by quenching with other species, namely N_2 and O_2 molecules.[72] However, according to OES analyses, this latter process may not be of major importance in the preparation of the present set of oxynitrides since these two reactive gases were not detected in the plasma, and the intensity of Ar lines decreases very slightly as the N_2+O_2 partial pressure increases (FIG. 4). By its turn, the double peak of Al decreases sharply with the increase of the N_2+O_2 partial pressure, as observed in FIG. 4. This behavior is in agreement with the target poisoning effect, since the formation of nitrides and oxides at the target's surface reduces its sputtering yield. On the other hand, the increase of the electron secondary emission explains the low target voltage previously observed (FIG. 2).

At this point, according to the OES analyses, it seems clear that the target poisoning is an important factor affecting the plasma composition. It is also important to understand how the plasma parameters are affected by the observed trends, namely how they are influenced by the partial pressure of the reactive gas and what is the role of the target condition.

C. Determination of the plasma parameters using a floating probe

1. Electron temperature and ion flux near the cathode

The electron temperature (T_e) and the ion flux (Γ^+) were calculated based on the method described in section II.B.2. and are displayed in FIG. 5(a-b), for partial pressures of N_2+O_2 up to 5.6×10^{-2} Pa. The floating probe was placed at 18 mm from the target and in front of the erosion track. The results were obtained by applying a sinusoidal wave to the probe, whose applied frequencies (f) and amplitudes (V_0) are indicated in FIG. 5, along with the resistor value.

FIG. 5(a) shows a gradual increase of the electron temperature near the cathode, as the N_2+O_2 partial pressure is increased. This trend can be explained, again, based on the ion induced secondary electron emission yield ($\gamma_{eff.}$) variation. Indeed, as discussed before, the gradual decrease of the target potential was mainly due to the rise of $\gamma_{eff.}$ coefficient. It varies between the

value of the pure Al and those of Al_2O_3 or AlN, depending on the fractions of the target covered by oxides and/or nitrides. The rise of the $\gamma_{eff.}$ coefficient means that the number of electrons emitted per incident ion increases, which enhances the population of secondary high energy electrons accelerated in the plasma direction.

This enhancement of the flux of secondary electrons from the target also explains the decrease of the ion flux, FIG. 5(b). Since the power supply is controlled by the current, the increase of the electron flux from the target is compensated by a decrease of the ion current in its vicinity, thus explaining the evolution of the ion flux as a function of the reactive gas partial pressure.

The plasma density (n_i) for the Ar discharge was also estimated using Eqs. 3 and 4. The obtained value was 2×10^{11} cm^{-3}, which is a typical value for this kind of plasmas.[73] A smooth decrease of the plasma density was observed as the N_2+O_2 partial pressure was increased, which is a direct consequence of the evolution of the electron temperature and ion flux. For these calculations it was assumed that the ion mass (M_i) in the Bohm velocity (Eq. 4) is approximately equal to the Ar mass, although some residual nitrogen and oxygen could be present.

2. Electron temperature and ion flux near the substrate

The plasma parameters were also estimated in a region away from the target, about 22 mm from the substrate. The results of the electron temperature and ion flux as a function of the N_2+O_2 partial pressure are plotted in FIG. 6(a-b). The electron temperature, FIG. 6(a), increases from a value of about 1.9 eV, for a pure Ar discharge, up to a value of 3.6 eV, corresponding to a N_2+O_2 partial pressure of 5.6×10^{-2} Pa. The ion flux suffers a smooth increase of about 25 %. The results presented in FIG. 6(a-b) suggest some electron and ion bombardments on the substrate, as expected due to the magnetron configuration (type-2 unbalanced magnetron).[27] The increase of T_e is again related to the enhancement of secondary electron population, caused by the increase of the flux of secondary electrons due to the gradual poisoning of the target as the partial pressure of reactive species increases. The increase of the electron temperature T_e induces also an increase of the Bohm velocity of the ions and this also explains the behavior of the ion flux, FIG. 6(b).

The plasma density was also calculated for the Ar discharge near the substrate. Its value was about half the value estimated near the cathode: 2×10^{11} cm^{-3} near the target, and 0.9×10^{11} cm^{-3}

near the substrate. This decrease was expected since in magnetron discharges the plasma density is higher in the vicinity of the racetrack of the target.[74,75]

D. The prepared thin films characteristics

RBS analysis revealed uniform composition across the film thickness. The compositions of the deposited films are presented in TABLE II along with their thickness determined by SEM.

It is widely accepted that the processing conditions strongly influence the intrinsic properties (composition, microstructure, grain orientation, etc.) and the functional properties (optical, mechanical, electrical, etc.) of the deposited films, but it is also true that is difficult to distinguish the influence of each deposition parameter on those properties.[45] Actually, a change in a single external parameter, such as the partial pressure of reactive gases (N_2+O_2 in the present case), is capable of changing several discharge parameters and the plasma characteristics, as demonstrated above. The changes observed in the target potential, plasma composition and plasma parameters are likely to induce different compositions and bonding characteristics, as well as different microstructures. Concerning the structure and morphology, and beyond the fundamental processes of films' growth, revised by Petrov et al., [76] there are other factors to take into account. The deposition rate, the substrate temperature and, mostly important, the fluxes on the substrate (metallic flux, energy flux, ion flux, etc.)[45] are certainly important parameters to be considered. In particular, the microstructure of the films is strongly influenced by the surface mobility of the incoming particles or the temperature of the growing surface,[77] and thus being quite sensitive to the change in all the above parameters.

The temperature of the growing film is difficult to estimate and can be very different from the temperature usually measured - the substrate temperature -, since it is the film that effectively is exposed to the particle bombardment.[78] Taking this point into consideration, it is accepted that the temperature of the growing film can be affected by the (i) the substrate heating,[79] (ii) the energy dissipated by vapor condensation[80] and (iii) the energy flux of particles arriving to the substrate.[45] By its turn, the energy flux depends on the particles (atoms, ions, electrons) that impinge on the substrate and on the kinetic energy of each of these particles.[45,79]

The substrate temperature and the deposition (or growth) rate of the films are plotted as a function of the partial pressure of N_2+O_2 (FIG. 7).

This figure shows that the substrate temperature (initially at 80 ºC, before discharge ignition) stabilizes at approximately 250 ºC for a pure Ar discharge and remains roughly constant

for reactive gas partial pressure up to 1×10^{-2} Pa. In this range of pressures, the deposition rate is approximately constant (~ 35-37 $nm.min^{-1}$) and the films reveal a typical columnar-like growth, as it can be observed from the cross-section SEM micrographs embedded in FIG. 7 (zone I). As the reactive gas partial pressure increases, the substrate temperature sharply decreases to values below 175 ºC, tending to ~160 ºC for higher pressures. On the contrary, the growth rate increases on passing from zone I towards the zone labeled as zone T (transition zone), gradually decreasing thereafter from about 42 $nm.min^{-1}$ towards 21 $nm.min^{-1}$. This behavior is consistent with the changes observed in the type of growth, since the films indexed to zone T revealed a granular structure separated by voids (cauliflower-type), which is known to increase the roughness and porosity and hence decreases the films' density,[77] contrarily to the less voided structure found for the films indexed to zone I. The films deposited with the target in the regime II, reveal a growth rate of approximately 5 $nm.min^{-1}$. These films are also dense and exhibit a more compact microstructure, being indexed to zone II, as observed in FIG. 7 where it's embedded a SEM image of a representative sample.

Assuming that the substrate temperature is directly connected to the temperature of the growing film, one can consider similar trends for both quantities. On the other hand, since the energy of the most energetic particles that arrive to the substrate (mainly Ar^+ and Al atoms) are not known, it's difficult to distinguish each contribution to the film's temperature. According to FIG. 6, the ion flux, and hence the electron flux, increase towards the substrate as the reactive gas partial pressure rises and thus this should lead to an increase of the substrate temperature. Nevertheless, this was not observed. In order to explain the observed behavior one has to regard the OES results, FIGs. 3 and 4. As discussed before, the increase of the N_2+O_2 partial pressure induced a gradual poisoning of the target and thus a reduction of its sputtering yield, which lead to a sharp decrease of the Al peak intensity. This indicates a strong decrease of the flux of Al atoms arriving to the substrate and of the energy transferred to the latter, which is a plausible explanation for the temperature evolution. According to S. Mahieu [45], the three components: metal flux, electron flux (condensation + kinetic energy) and ion flux have similar contributions to the thermal heating of the substrate under grounded conditions. In the present case, the measured increase of ion flux to the substrate is only of 25%, the same increase is expected for electron flux, while a sharp reduction of the metal flux to the substrate is suggested by the Al line intensity evolution (FIG. 4), which thus constitutes the most plausible explanation for the substrate temperature

evolution. Furthermore, the reduction of the amount of Al atoms arriving to the substrate also explains the decrease of the growth rate of the films.

The lower temperatures also reduce the atoms mobility in the film's surface and this can be one of the factors explaining the microstructure of some films. The observed microstructure in the films indexed to zone T is in agreement with *zone Ia* of the Mahieu and Depla structure zone model (SZM), which is an extension to the well-know Thornton model[77] According to this SZM, the low mobility of the atoms favors a hit and stick (or ballistic) growth, which can induce voided and columnar structures.

The other major factor contributing to the microstructural changes is obviously the increase of reactive species, especially oxygen, which is known to inhibit the grain coarsening during coalescence and film growth.[76] In fact, as shown in FIG. 8, the rise of the N_2+O_2 partial pressure induces the increase of non-metallic elements concentration and hence a wide range of chemical compositions, such as the formation of substoichiometric AlN_xO_y films with atomic ratios gradually increasing up to 0.8, as well as an abrupt change in the films' composition in zone II, where close-stoichiometric Al_2O_3 (alumina) films were formed.[39] The formation of close-stoichiometric alumina films with nitrogen concentration below 5 at.% occurs for N_2+O_2 partial pressure of 5.6×10^{-2} Pa and above. The observed Al-type structure in zone I is gradually disappearing in zone T, until a complete amorphization is obtained in zone II, due to the formation of close-stoichiometric aluminum oxide (Al_2O_3) films (see diffractograms in FIG. 8).[40]

According to the overall set of results one can claim that the change of a single external parameter, such as the reactive gas partial pressure, strongly affects the processing conditions (target potential, plasma composition and plasma parameters). It was actually demonstrated that not only the composition of the films is affected by the increase of reactive species, but also their microstructural features, due to changes in the discharge conditions. Furthermore, the different composition, as well as the structural and morphological features, induced different properties, tailored among those of pure Al, AlN and Al_2O_3.

The diagram represented in FIG. 9 resumes the results discussed above as well as the major findings of this work in terms of electrical and optical behaviors of the films, discussed in recent papers.[39,40] As it can be observed, the change of the N_2+O_2 partial pressure affects many discharge parameters, such as the target potential (U_{targ}), the plasma parameters, the electron temperature (T_e) and the ion flux (Γ^+), as well as the substrate temperature (T_{subs}). The particular combination

of the mentioned parameters induced the formation of films with different compositions and microstructural features, such as a transition from polycrystalline Al-type films towards nanocomposite-like materials, where Al nanoparticles are dispersed in an amorphous semiconducting/insulator matrix, or even the production of dense and amorphous Al_2O_3 films.

The electrical behavior of the films varied from metallic-like in zone I, towards a transition behavior, explained taking into consideration the structural arrangement proposed for the films, in zone T, ending up as insulator-type in zone II where Al_2O_3 was produced.[39] While the electrical resistivity (ρ) of the sub-stoichiometric films ($C_{N+O}/C_{Al} < 0.8$) increased up to four orders of magnitude above the aluminum film, their temperature coefficient of resistance (TCR_{300K}) changed from positive to negative values. The electrical behavior of the films was explained taking into account the morphology of the films, which are composed of aluminum nanoparticles dispersed in a semiconductor or insulator matrix, forming a percolating network. In this case, the TCR has two components: the conductive component, due to the Al nanoparticles, and the barrier component due to the matrix. Since the barrier component has a negative dependence with the temperature, the enlargement of the matrix, due to the increase of the non-metallic elements concentration, explains the negative TCR values found for some films.[39]

The optical behavior ranged from the typical profile of polycrystalline aluminum (zone I) towards an unusual reflectance profile, characterized by values as low as 5% and nearly independent of the wavelength (zone T).[40] This optical profile was again associated to the morphology of the films, since it is known that a network of nanoparticles dispersed in a dielectric matrix can induce a broadband optical absorption.[81] The films indexed to zone II revealed interference-like colorations, consistent with their semi-transparency.[38]

IV Conclusions

In this work, some discharge parameters were monitored during the deposition of AlN_xO_y films by reactive DC magnetron sputtering. It was used Ar as working gas, with a fixed partial pressure of 3×10^{-1} Pa, and a reactive gas mixture composed of N_2+O_2 (17:3 ratio). The intended change of the partial pressure of reactive gas (N_2+O_2) influenced the target condition and the plasma parameters which, altogether, affected the substrate temperature and deposition characteristics.

The target was strongly affected by the N_2+O_2 partial pressure, which caused the gradual coverage of its surface with nitrides and oxides, thus affecting the cathode potential and its sputtering yield, with consequences in the flux of Al atoms towards the substrate, as demonstrated by OES analysis. Furthermore, it was not detected the presence of both reactive gases in the plasma, meaning that they must be essentially consumed by the chamber's surfaces, namely in the substrates during film deposition and in chamber walls, beyond the target.

The target poisoning effect is also one of the main factors controlling the discharge characteristics and hence the changes observed in the plasma parameters. In fact, it was observed that the ion flux near the target decreased with the increase of the partial pressure of N_2+O_2. Therefore, the flux of secondary electrons emitted from the target should increase, since the target current density was a fixed external parameter. This statement is in agreement with the increase of the secondary electron emission yield, which was used to explain the gradual decrease of the target potential. The slight increase of the electron temperature near the target is also in agreement with these features, since the increase of secondary electrons emitted from the target enhances the population of high energy electrons in the plasma.

The substrate temperature suffered a sharp decrease with the increase of the partial pressure of the reactive gas. Since the flux of ions and electrons near the substrate increased with the N_2+O_2 partial pressure, the evolution of the substrate temperature was attributed mainly to the reduction of the number of Al atoms arriving to the substrate.

The particular discharge conditions used to produce the AlN_xO_y films induced not only a range of chemical compositions, due to the increase of reactive species (oxygen and nitrogen), but also important changes in the bonding states and microstructural characteristics, which explained the observed electrical and optical responses of the deposited films.

Acknowledgements

This research was supported by FEDER through the COMPETE Program and by the Portuguese Foundation for Science and Technology (FCT) in the framework of the Strategic Project PEST-C/FIS/UI607/2011. J. Borges also acknowledges FCT financial support under PhD grant Nº SFRH/BD/47118/2008 (*financiado por POPH – QREN – Tipologia 4.1 – Formação Avançada, comparticipado pelo Fundo Social Europeu e por fundos nacionais do MCTES)*.

References

[1]M. Ohring, *Material Science of Thin Films (Deposition & Structure)* (Academic Press, 2002).
[2]F. Vaz, L. Rebouta, M. Andritschky, M. F. da Silva, and J. C. Soares, Surface and Coatings Technology **98,** 912 (1998).
[3]D. Munteanu, C. Ionescu, C. Olteanu, A. Munteanu, F. Davin, L. Cunha, C. Moura, and F. Vaz, Wear **268,** 552 (2010).
[4]J. Borges, C. Fonseca, N. P. Barradas, E. Alves, T. Girardeau, F. Paumier, F. Vaz, and L. Marques, Electrochimica Acta **106,** 23 (2013).
[5]C. Fernandes, S. Carvalho, L. Rebouta, F. Vaz, M. F. Denannot, J. Pacaud, J. P. Riviére, and A. Cavaleiro, Vacuum **82,** 1470 (2008).
[6]N. M. G. Parreira, N. J. M. Carvalho, F. Vaz, and A. Cavaleiro, Surface and Coatings Technology **200,** 6511 (2006).
[7]E. Ribeiro, L. Rebouta, S. Carvalho, F. Vaz, G. G. Fuentes, R. Rodriguez, M. Zazpe, E. Alves, P. Goudeau, and J. P. Rivière, Surface and Coatings Technology **188–189,** 351 (2004).
[8]P. Carvalho, F. Vaz, L. Rebouta, S. Carvalho, L. Cunha, P. Goudeau, J. P. Rivière, E. Alves, and A. Cavaleiro, Surface and Coatings Technology **200,** 748 (2005).
[9]M. Torrell, L. Cunha, A. Cavaleiro, E. Alves, N. P. Barradas, and F. Vaz, Applied Surface Science **256,** 6536 (2010).
[10]C. Lopes, C. Gonçalves, P. Pedrosa, F. Macedo, E. Alves, N. P. Barradas, N. Martin, C. Fonseca, and F. Vaz, Applied Surface Science.
[11]P. Carvalho, J. M. Chappe, L. Cunha, S. Lanceros-Mendez, P. Alpuim, F. Vaz, E. Alves, C. Rousselot, J. P. Espinos, and A. R. Gonzalez-Elipe, Journal of Applied Physics **103,** 104907 (2008).
[12]R. F. Gibson, Composite Structures **92,** 2793 (2010).
[13]S. Nemat-Nasser, S. Nemat-Nasser, T. Plaisted, A. Starr, and A. V. Amirkhizi, in *Biomimetics: Biologically Inspired Technologies*, edited by Y. Bar-Cohen (CRC Press, 2005).
[14]A. C. Fernandes, P. Carvalho, F. Vaz, S. Lanceros-Méndez, A. V. Machado, N. M. G. Parreira, J. F. Pierson, and N. Martin, Thin Solid Films **515,** 866 (2006).
[15]I. Safi, Surface and Coatings Technology **127,** 203 (2000).
[16]J. Musil, P. Baroch, J. Vlček, K. H. Nam, and J. G. Han, Thin Solid Films **475,** 208 (2005).
[17]G. Bräuer, B. Szyszka, M. Vergöhl, and R. Bandorf, Vacuum **84,** 1354 (2010).
[18]C. A. Bishop, in *Vacuum Deposition onto Webs, Films and Foils (Second Edition)*, edited by C. A. Bishop (William Andrew Publishing, Oxford, 2011), p. 375.
[19]R. De Gryse, J. Haemers, W. P. Leroy, and D. Depla, Thin Solid Films **520,** 5833 (2012).
[20]W. D. Sproul, Science **273,** 889 (1996).
[21]R. Franchy, Surface Science Reports **38,** 195 (2000).
[22]F. Vaz, P. Machado, L. Rebouta, J. A. Mendes, S. Lanceros-Méndez, L. Cunha, S. M. C. Nascimento, P. Goudeau, J. P. Rivière, E. Alves, and A. Sidor, Thin Solid Films **420–421,** 421 (2002).
[23]J. M. Ngaruiya, O. Kappertz, S. H. Mohamed, and M. Wuttig, Applied Physics Letters **85,** 748 (2004).
[24]P. Carvalho, F. Vaz, L. Rebouta, S. Carvalho, L. Cunha, P. Goudeau, J. P. Riviere, E. Alves, and A. Cavaleiro, Surface and Coatings Technology **200,** 748 (2005).
[25]M. T. Mathew, E. Ariza, L. A. Rocha, F. Vaz, A. C. Fernandes, and M. M. Stack, Electrochimica Acta **56,** 929 (2010).
[26]M. Torrell, P. Machado, L. Cunha, N. M. Figueiredo, J. C. Oliveira, C. Louro, and F. Vaz, Surface and Coatings Technology **204,** 1569 (2010).
[27]P. J. Kelly and R. D. Arnell, Vacuum **56,** 159 (2000).
[28]F. Vaz, N. Martin, and M. Fenker, *Metallic Oxynitride Thin Films by Reactive Sputtering and Related Deposition Methods* (Bentham Science Publishers, 2013).
[29]N. Martin, O. Banakh, A. M. E. Santo, S. Springer, R. Sanjinés, J. Takadoum, and F. Lévy, Applied Surface Science **185,** 123 (2001).

[30]F. Vaz, P. Cerqueira, L. Rebouta, S. M. C. Nascimento, E. Alves, P. Goudeau, J. P. Riviere, K. Pischow, and J. de Rijk, Thin Solid Films **447-448,** 449 (2004).
[31]O. Banakh, P. A. Steinmann, and L. Dumitrescu-Buforn, Thin Solid Films **513,** 136 (2006).
[32]M. Fenker, H. Kappl, O. Banakh, N. Martin, and J. F. Pierson, Surface and Coatings Technology **201,** 4152 (2006).
[33]S. Venkataraj, D. Severin, S. H. Mohamed, J. Ngaruiya, O. Kappertz, and M. Wuttig, Thin Solid Films **502,** 228 (2006).
[34]N. M. G. Parreira, T. Polcar, N. Martin, O. Banakh, and A. Cavaleiro, Plasma Processes and Polymers **4,** S69 (2007).
[35]M. Fenker, H. Kappl, P. Carvalho, and F. Vaz, Thin Solid Films **519,** 2457 (2011).
[36]R. Arvinte, J. Borges, R. E. Sousa, D. Munteanu, N. P. Barradas, E. Alves, F. Vaz, and L. Marques, Applied Surface Science **257,** 9120 (2011).
[37]J. Borges, F. Vaz, and L. Marques, Applied Surface Science **257,** 1478 (2010).
[38]J. Borges, E. Alves, F. Vaz, and L. Marques, in *Optical properties of AlNxOy thin films deposited by DC magnetron sputtering*, Braga, 2011 (SPIE), p. 80010F.
[39]J. Borges, N. Martin, N. P. Barradas, E. Alves, D. Eyidi, M. F. Beaufort, J. P. Riviere, F. Vaz, and L. Marques, Thin Solid Films **520,** 6709 (2012).
[40]J. Borges, N. P. Barradas, E. Alves, M. F. Beaufort, D. Eyidi, F. Vaz, and L. Marques, Journal of Physics D: Applied Physics **46,** 015305 (2013).
[41]J. Borges, N. P. Barradas, E. Alves, N. Martin, M. F. Beaufort, S. Camelio, D. Eyidi, T. Girardeau, F. Paumier, J. P. Riviere, F. Vaz, and L. Marques, in *Metallic Oxynitride Thin Films by Reactive Sputtering and Related Deposition Methods*, edited by F. Vaz, N. Martin, and M. Fenker (Bentham Science Publishers, 2013), p. 195.
[42]N. D. Corbin, Journal of the European Ceramic Society **5,** 143 (1989).
[43]A. Pallone, J. Demaree, and J. Adams, Nuclear Instruments and Methods in Physics Research Section B: Beam Interactions with Materials and Atoms **219-220,** 755 (2004).
[44]J. J. Guo, K. Wang, T. Fujita, J. W. McCauley, J. P. Singh, and M. W. Chen, Acta Materialia **59,** 1671 (2011).
[45]S. Mahieu and D. Depla, Journal of Physics D: Applied Physics **42,** 053002 (2009).
[46]M.-H. Lee, S.-H. Jang, and C.-W. Chung, Journal of Applied Physics **101,** 033305 (2007).
[47]J. A. Boedo, D. Gray, R. W. Conn, P. Luong, M. Schaffer, R. S. Ivanov, A. V. Chernilevsky, G. V. Oost, and T. Team, Review of Scientific Instruments **70,** 2997 (1999).
[48]Y.-K. Lee, J.-H. Ku, and C.-W. Chung, Plasma Sources Science and Technology **20,** 015005 (2011).
[49]Y.-D. Kim, Y.-S. Kim, H.-C. Lee, J.-Y. Bang, and C.-W. Chung, Physics of Plasmas **18,** 033508 (2011).
[50]U. Fantz, Plasma Sources Science and Technology **15,** S137 (2006).
[51]D. Mariotti, Y. Shimizu, T. Sasaki, and N. Koshizaki, Applied Physics Letters **89,** 201502 (2006).
[52]X.-M. Zhu, W.-C. Chen, J. Li, and Y.-K. Pu, Journal of Physics D: Applied Physics **42,** 025203 (2009).
[53]J. B. Boffard, R. O. Jung, C. C. Lin, and A. E. Wendt, Plasma Sources Science and Technology **19,** 065001 (2010).
[54]X.-M. Zhu and Y.-K. Pu, Journal of Physics D: Applied Physics **43,** 403001 (2010).
[55]N. P. Barradas, C. Jeynes, and R. P. Webb, Applied Physics Letters **71,** 291 (1997).
[56]A. Ruhm, B. P. Topeverg, and H. Dosch, Physical Review B **60,** 16073 (1999).
[57]D. Depla, G. Buyle, J. Haemers, and R. De Gryse, Surface and Coatings Technology **200,** 4329 (2006).
[58]D. Depla, S. Mahieu, and R. De Gryse, Thin Solid Films **517,** 2825 (2009).
[59]D. Depla, J. Haemers, and R. De Gryse, Thin Solid Films **515,** 468 (2006).
[60]D. Depla and R. D. Gryse, Plasma Sources Science and Technology **10,** 547 (2001).
[61]D. Depla and R. De Gryse, Surface and Coatings Technology **183,** 190 (2004).
[62]D. Depla and R. De Gryse, Surface and Coatings Technology **183,** 184 (2004).
[63]J. Schulte and G. Sobe, Thin Solid Films **324,** 19 (1998).
[64]D. Depla, S. Heirwegh, S. Mahieu, J. Haemers, and R. D. Gryse, Journal of Applied Physics **101,** 013301 (2007).

[65]R. Mientus and K. Ellmer, Surface and Coatings Technology **116-119,** 1093 (1999).
[66]S. Venkataraj, D. Severin, R. Drese, F. Koerfer, and M. Wuttig, Thin Solid Films **502,** 235 (2006).
[67]D. Depla, H. Tomaszewski, G. Buyle, and R. De Gryse, Surface and Coatings Technology **201,** 848 (2006).
[68]K. Koski, J. Hölsä, and P. Juliet, Surface and Coatings Technology **115,** 163 (1999).
[69]A. Anders, Thin Solid Films **502,** 22 (2006).
[70]M. F. Dony, A. Ricard, J. P. Dauchot, M. Hecq, and M. Wautelet, Surface and Coatings Technology **74-75, Part 1,** 479 (1995).
[71]X.-M. Zhu and Y.-K. Pu, Plasma Sources Science and Technology **17,** 024002 (2008).
[72]N. Sadeghi, D. W. Setser, A. Francis, U. Czarnetzki, and H. F. Dobele, The Journal of Chemical Physics **115,** 3144 (2001).
[73]E. Bultinck, S. Mahieu, D. Depla, and A. Bogaerts, New Journal of Physics **11,** 023039 (2009).
[74]C. Costin, L. Marques, G. Popa, and G. Gousset, Plasma Sources Science and Technology **14,** 168 (2005).
[75]S.-H. Seo, J.-H. In, and H.-Y. Chang, Plasma Sources Science and Technology **15,** 256 (2006).
[76]I. Petrov, P. B. Barna, L. Hultman, and J. E. Greene, Journal of Vacuum Science & Technology A: Vacuum, Surfaces, and Films **21,** S117 (2003).
[77]S. Mahieu, P. Ghekiere, D. Depla, and R. De Gryse, Thin Solid Films **515,** 1229 (2006).
[78]L. R. Shaginyan, V. R. Shaginyan, and J. G. Han, The European Physical Journal B - Condensed Matter and Complex Systems **46,** 335 (2005).
[79]H. Kersten, H. Deutsch, H. Steffen, G. M. W. Kroesen, and R. Hippler, Vacuum **63,** 385 (2001).
[80]M. Ohring, *Materials Science of Thin Films: Deposition and Structure* (Academic Press, 2002).
[81]A. Biswas, H. Eilers, J. F. Hidden, O. C. Aktas, and C. V. S. Kiran, Applied Physics Letters **88,** 013103 (2006).

TABLES

TABLE I. Emission lines detected in the Ar/(N_2+O_2) discharge.

Species	Wavelength transition /nm	Transition
Al I	394.40	$^2P^0_{1/2} - {}^2S_{1/2}$
	396.15	$^2P^0_{3/2} - {}^2S_{1/2}$
Ar I	706.72	$4p(2p_3) \rightarrow 4s\ (1s_5)$
	738.40	$4p(2p_3) \rightarrow 4s\ (1s_4)$
	750.39	$4p(2p_1) \rightarrow 4s\ (1s_2)$
	751.47	$4p(2p_5) \rightarrow 4s\ (1s_4)$
	763.51	$4p(2p_6) \rightarrow 4s\ (1s_5)$
	772.38	$4p(2p_7) \rightarrow 4s\ (1s_5)$
	772.42	$4p(2p_2) \rightarrow 4s\ (1s_3)$
	794.82	$4p(2p_4) \rightarrow 4s\ (1s_3)$
	800.62	$4p(2p_6) \rightarrow 4s\ (1s_4)$
	801.48	$4p(2p_8) \rightarrow 4s\ (1s_5)$
	810.37	$4p(2p_7) \rightarrow 4s\ (1s_4)$
	811.53	$4p(2p_9) \rightarrow 4s\ (1s_5)$
	840.82	$4p(2p_3) \rightarrow 4s\ (1s_2)$
	842.47	$4p(2p_8) \rightarrow 4s\ (1s_4)$

TABLE II. Composition and thickness of the deposited AlN_xO_y films.

Zone	Partial pressure of N_2+O_2 (Pa)	Stoichiometry	Thickness / μm
Zone M	0.0	Al	3.4
	1.0×10^{-2}	$AlN_{0.04}O_{0.01}$	3.1
Zone T	2.4×10^{-2}	$AlN_{0.17}O_{0.14}$	3.7
	3.5×10^{-2}	$AlN_{0.26}O_{0.31}$	3.2
	4.0×10^{-2}	$AlN_{0.36}O_{0.30}$	2.3
	4.6×10^{-2}	$AlN_{0.40}O_{0.35}$	1.9
Zone II	5.6×10^{-2}	$Al_2O_{2.9}N_{0.4}$	0.46

Figure Captions

FIG. 1. Schematic diagram of the experimental setup of the floating probe.

FIG. 2. Behavior of the target potential as a function of the N_2+O_2 partial pressure. The partial pressure of Ar was kept constant (3×10^{-1} Pa).

FIG. 3. Optical emission spectra of representative Ar/(N_2+O_2) discharges (discharge current 75 $A.m^{-2}$). The partial pressure of Ar was kept constant (3×10^{-1} Pa).

FIG. 4. Evolution of the OES lines' intensity relatively to a pure Ar discharge, as a function of N_2+O_2 partial pressure.

FIG. 5. (a) Electron temperature (T_e) and (b) ion flux (Γ^+) as a function of the partial pressure of N_2+O_2. The probe was placed in front of the erosion track and 18 mm away from the target.

FIG. 6. (a) Electron temperature (T_e) and (b) ion flux (Γ^+) as a function of the N_2+O_2 partial pressure. The probe was placed close to the substrate (~22 mm).

FIG. 7. Equilibrium substrate temperature and growth rate of the deposited films as a function of the N_2+O_2 partial pressure. SEM images of representative films are displayed (the size of each image, width×height, is also labeled).

FIG. 8. Ratio between the concentration (at. %) of non-metallic elements over Al as a function of the reactive gas partial pressure. The evolution of the XRD peaks of the deposited films is also presented, showing an Al-type structure.

FIG. 9. Diagram resuming the major results of this work, in terms of discharge parameters and, as well, the characteristics and properties of the films deposited under those conditions. It can be observed the evolution of the morphology, the electrical resistivity at room temperature (ρ), the atomic ratio (C_{N+O}/C_{Al}), the electron temperature (T_e), the ion flux near the target (Γ^+), the target potential ($U_{targ.}$), the substrate temperature ($T_{subs.}$), the temperature coefficient of resistance (TCR_{300K}) and the optical behavior as a function of the partial pressure of the reactive gas (p (N_2+O_2)).

Figures

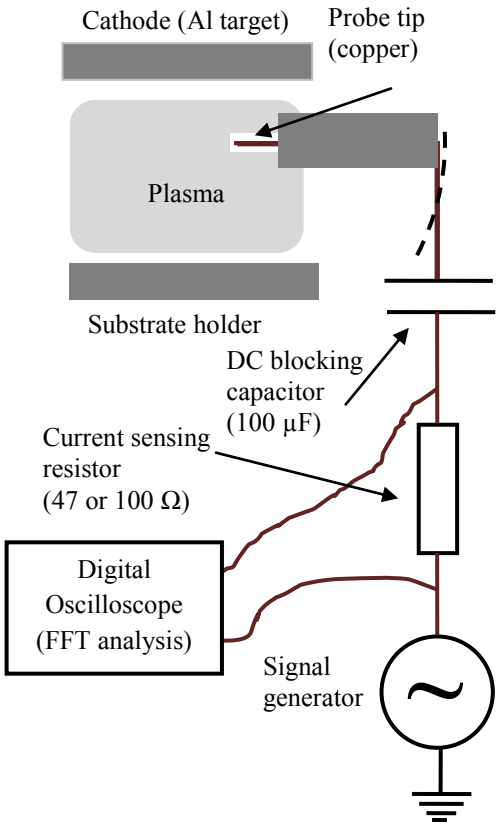

FIG. 1. Schematic diagram of the experimental setup of the floating probe.

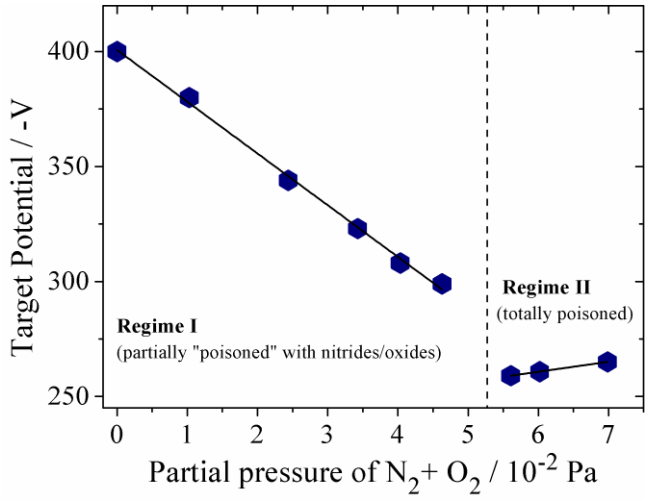

FIG. 2. Behavior of the target potential as a function of the N_2+O_2 partial pressure. The partial pressure of Ar was kept constant (3×10^{-1} Pa).

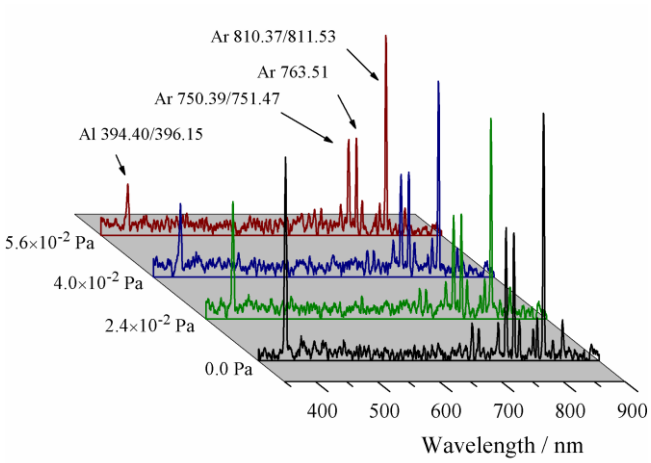

FIG. 3. Optical emission spectra of representative Ar/(N_2+O_2) discharges (discharge current 75 A.m^{-2}). The partial pressure of Ar was kept constant (3×10^{-1} Pa).

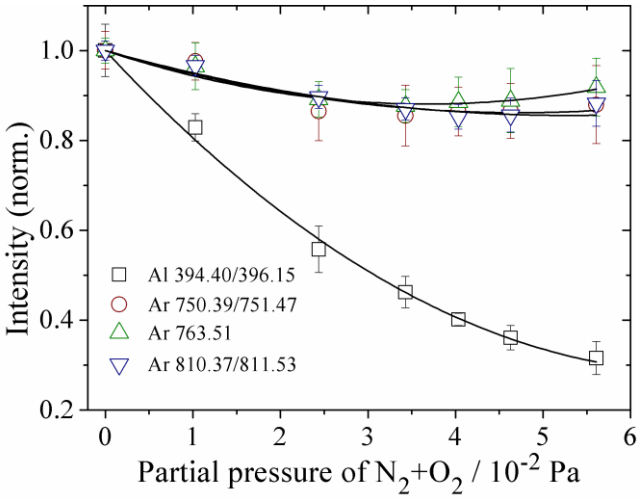

FIG. 4. Evolution of the OES lines' intensity relatively to the pure Ar discharge, as a function of N_2+O_2 partial pressure.

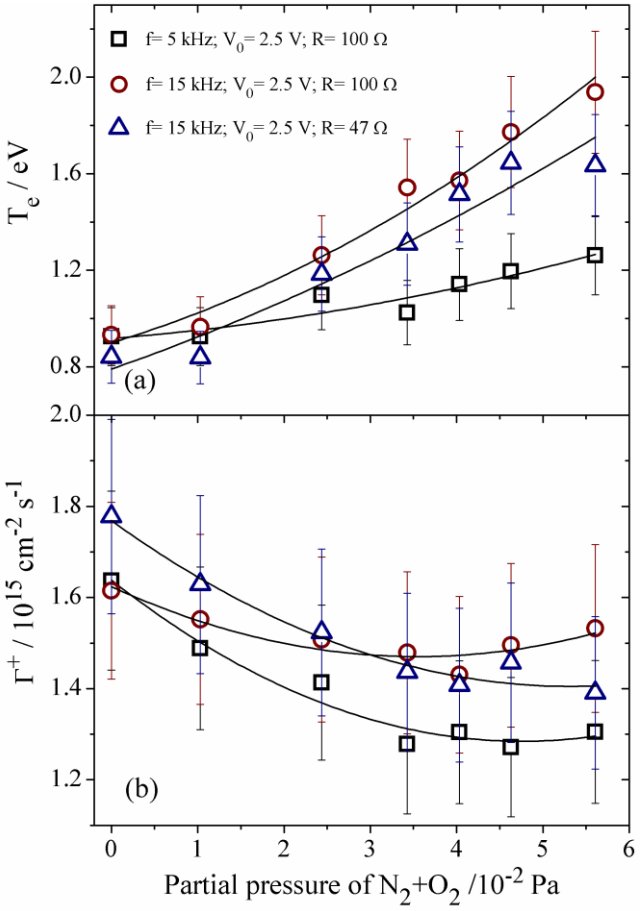

FIG. 5. (a) Electron temperature (T_e) and (b) ion flux (Γ^+) as a function of the partial pressure of N_2+O_2. The probe was placed in front of the erosion track and 18 mm away from the target.

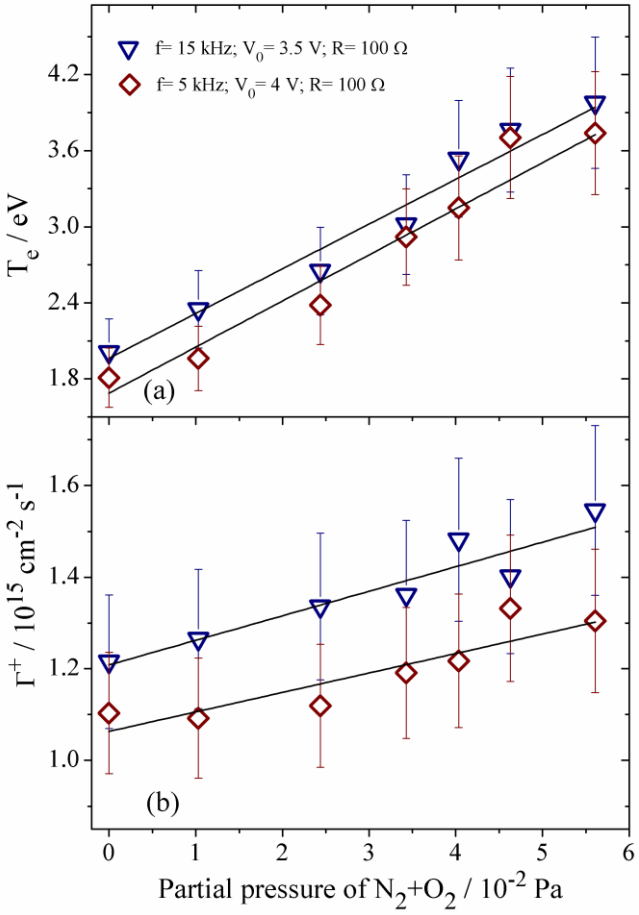

FIG. 6. (a) Electron temperature (T_e) and (b) ion flux (Γ^+) as a function of the N_2+O_2 partial pressure. The probe was placed close to the substrate (~22 mm).

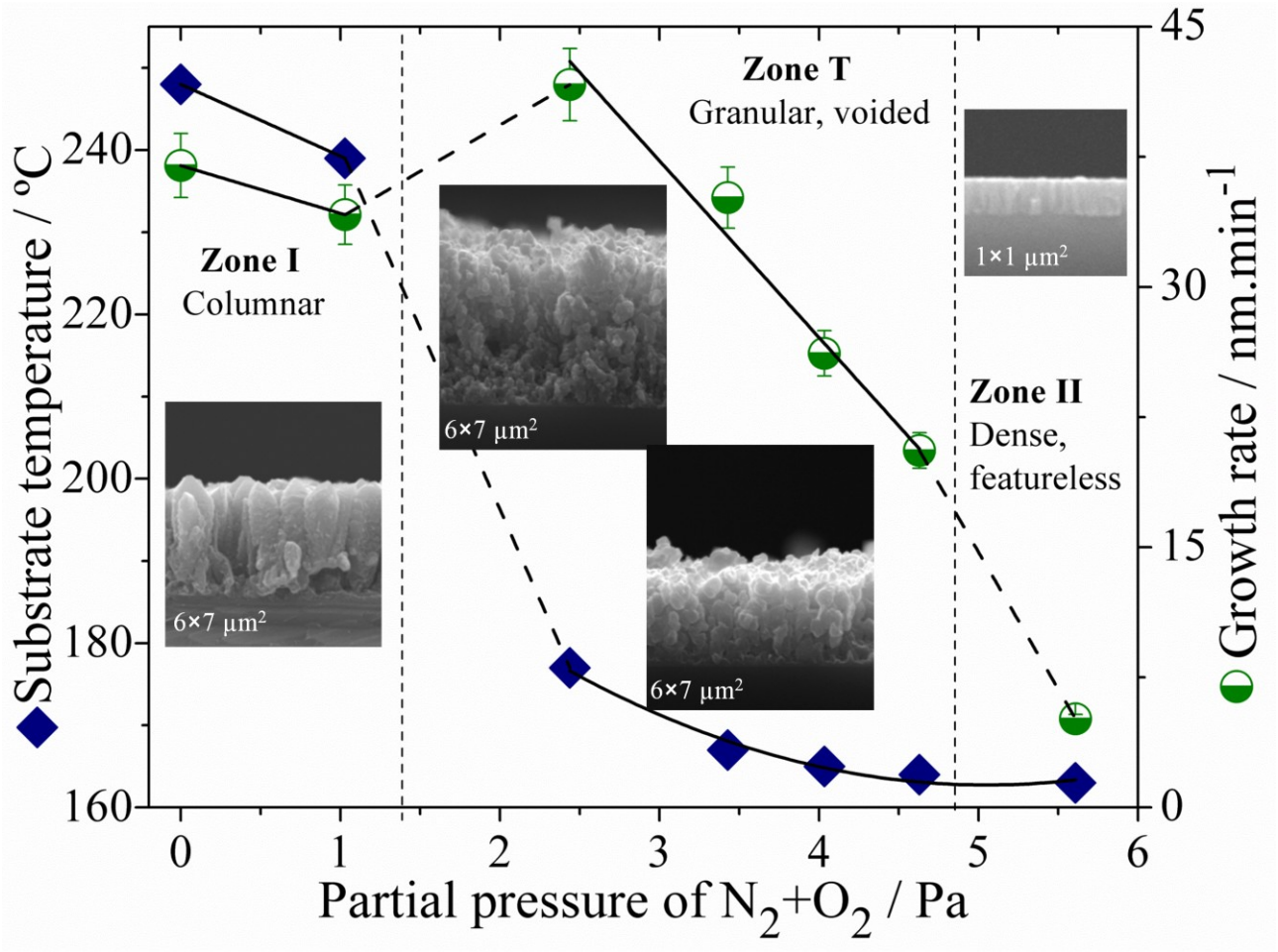

FIG. 7. Equilibrium substrate temperature and growth rate of the deposited films as a function of the N_2+O_2 partial pressure. SEM images of representative films are displayed (the size of each image, width×height, is also labeled).

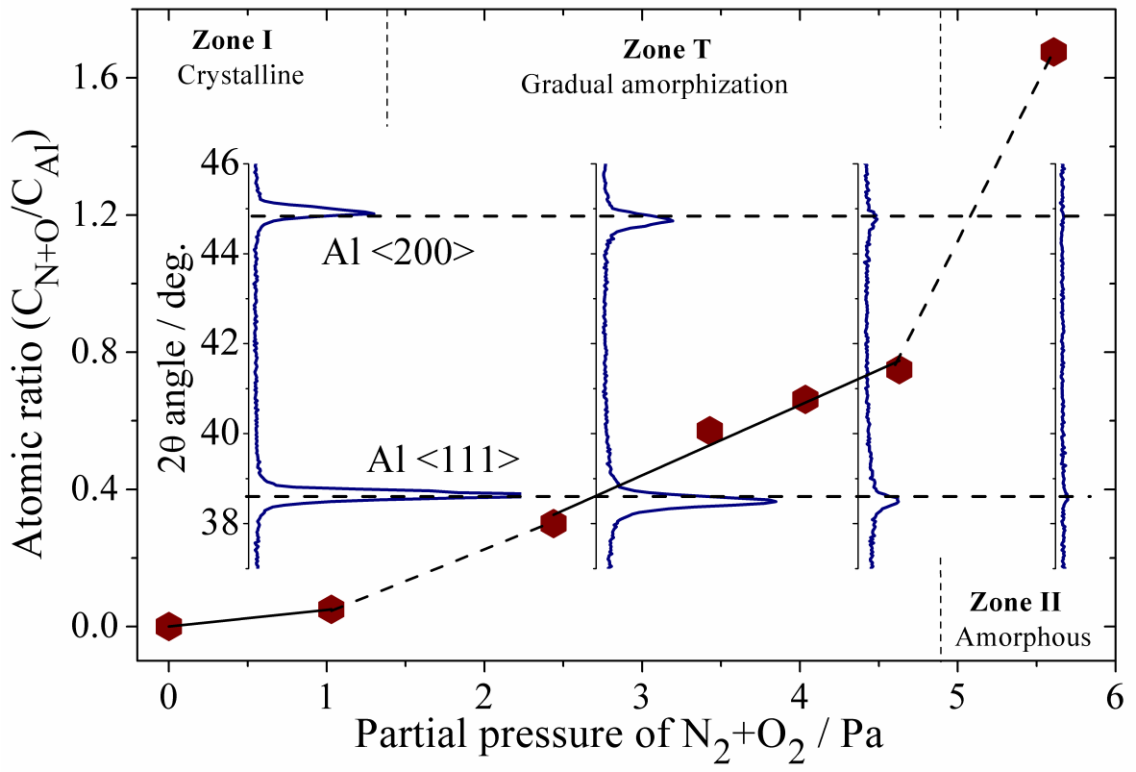

FIG. 8. Ratio between the concentration (at. %) of non-metallic elements over Al as a function of the reactive gas partial pressure. The evolution of the XRD peaks of the deposited films is also presented, showing an Al-type structure.

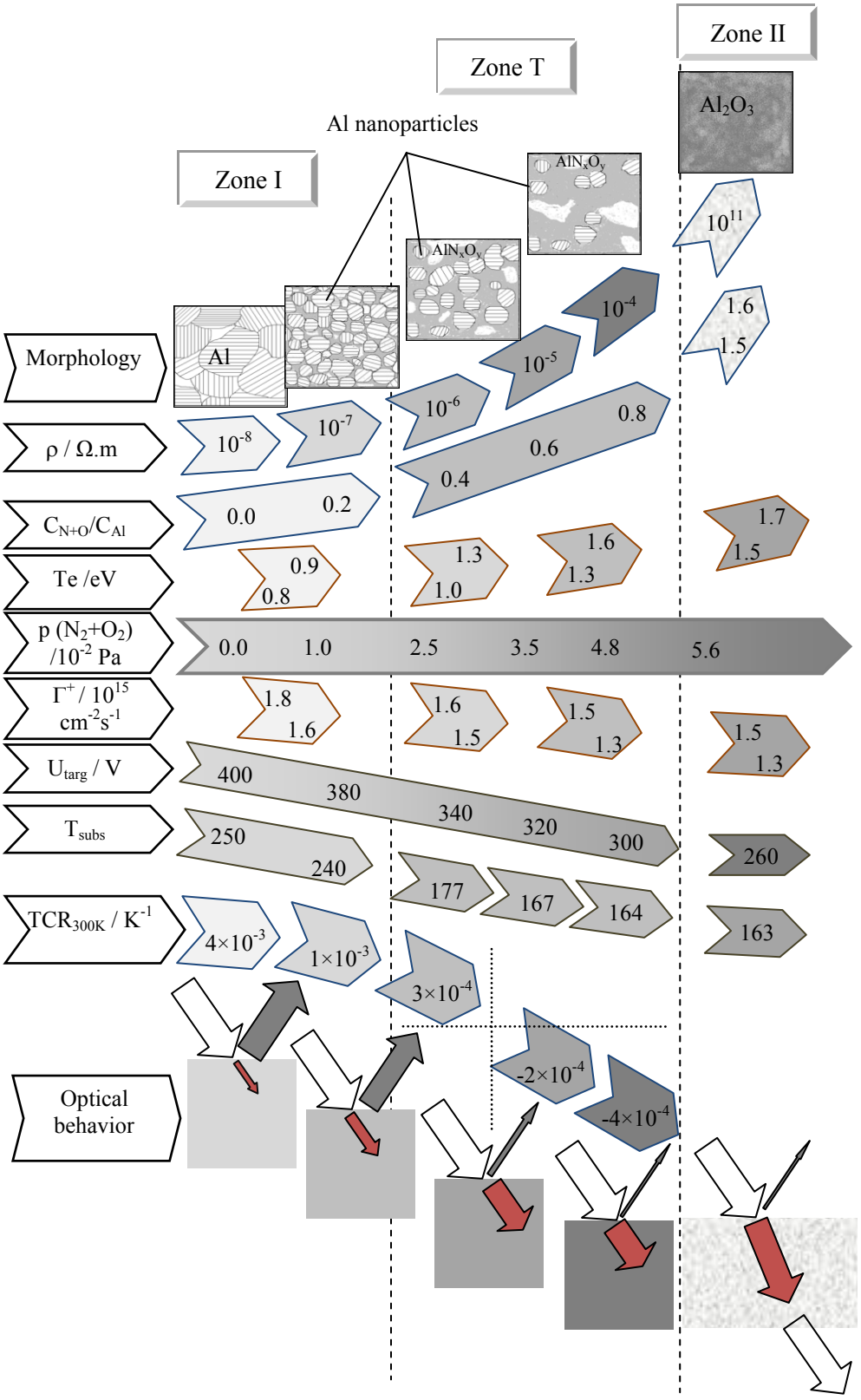
Zone I
Zone T
Zone II
Al nanoparticles
Al_2O_3
AlN_xO_y
AlN_xO_y
Al
Morphology
ρ / Ω.m
C_{N+O}/C_{Al}
Te /eV
p (N_2+O_2) /10^{-2} Pa
Γ^+ / 10^{15} $cm^{-2}s^{-1}$
U_{targ} / V
T_{subs}
TCR_{300K} / K^{-1}
Optical behavior
10^{11}
1.6
1.5
10^{-4}
10^{-5}
10^{-6}
10^{-7}
10^{-8}
0.8
0.6
0.4
0.2
0.0
1.7
1.5
1.6
1.3
1.3
1.0
0.9
0.8
0.0
1.0
2.5
3.5
4.8
5.6
1.8
1.6
1.6
1.5
1.5
1.3
1.5
1.3
400
380
340
320
300
260
250
240
177
167
164
163
4×10^{-3}
1×10^{-3}
3×10^{-4}
-2×10^{-4}
-4×10^{-4}

FIG. 9. Diagram resuming the major results of this work, in terms of discharge parameters and, as well, the characteristics and properties of the films deposited under those conditions. It can be observed the evolution of the morphology, the electrical resistivity at room temperature (ρ), the atomic ratio (C_{N+O}/C_{Al}), the electron temperature (T_e), the ion flux near the target (Γ^+), the target potential ($U_{targ.}$), the substrate temperature ($T_{subs.}$), the temperature coefficient of resistance (TCR_{300K}) and the optical behavior as a function of the partial pressure of the reactive gas (p (N_2+O_2)).